A general pattern of non-spiking neuron dynamics under the effect of potassium and calcium channel modifications

Loïs Naudin, Laetitia Raison-Aubry, Laure Buhry

A general pattern of non-spiking neuron dynamics under the effect of potassium and calcium channel modifications

Loïs Naudin[1*], Laetitia Raison-Aubry[1], and Laure Buhry[1*]

[1]Laboratoire Lorrain de Recherche en Informatique et ses Applications, CNRS, Université de Lorraine, Nancy, France

[*]Corresponding author: lois.naudin@gmail.com, laure.buhry@loria.fr

August 13, 2022

Abstract

Electrical activity of excitable cells results from ion exchanges through cell membranes, so that genetic or epigenetic changes in genes encoding ion channels are likely to affect neuronal electrical signaling throughout the brain. There is a large literature on the effect of variations in ion channels on the dynamics of spiking neurons that represent the main type of neurons found in the vertebrate nervous systems. Nevertheless, non-spiking neurons are also ubiquitous in many nervous tissues and play a critical role in the processing of some sensory systems. To our knowledge, however, how conductance variations affect the dynamics of non-spiking neurons has never been assessed. Based on experimental observations in the biological literature and on mathematical considerations, we first propose a phenotypic classification of non-spiking neurons. Then, we determine a general pattern of the phenotypic evolution of non-spiking neurons as a function of changes in calcium and potassium conductances. Furthermore, we study the homeostatic compensatory mechanisms of ion channels in a well-posed non-spiking retinal cone model. We show that there is a restricted range of ion conductance values for which the behavior and phenotype of the neuron are maintained.

Keywords: non-spiking neurons; conductance variations; bifurcation; retina; *Caenorhab-*

ditis elegans.

1 Introduction

Electrical activity of excitable cells results from ion flows through the cell membrane, such that genetic or epigenetic modifications of ion channel proteins are likely to affect electrical signaling throughout the brain. In particular, dysregulations of calcium and potassium channel functioning, and their possible impact on ion homeostasis, are implicated in a wide range of neurological and psychiatric disorders. Among them, we find neurodegenerative disorders such as Parkinson (Zhang et al., 2020; Hurley and Dexter, 2012), Huntington (Czeredys, 2020; Tong et al., 2014), or Alzheimer (Supnet and Bezprozvanny, 2010; Stutzmann, 2021; Villa et al., 2020) diseases, and various psychiatric diseases (Zhang et al., 2006; Heyes et al., 2015; Zamponi et al., 2015; Yanagi et al., 2014). Therefore, ion channel modifications are likely to affect sensory system processing as well, altering the electrical activity not only of spiking neurons, but also of non-spiking neurons as suggested by electrophysiological studies of retinal activity in patients suffering from Parkinson, Alzheimer, and Huntington diseases, epilepsy, depression, and schizophrenia (Silverstein et al., 2020).

While spiking neurons are thought to convey a large part of the neuronal information via action potential propagation along axons, non-spiking neurons, instead, modulate analog signals (*i.e.* graded potential responses). More specifically, the amplitude and waveform of the action potentials are essentially invariant with respect to the amplitude, duration, and waveform of the stimulus, unlike graded potentials whose waveform depends directly on the stimulus (Lockery et al., 2009) (Figure 1.A). This type of response has the advantage of preserving information content, but, as a consequence, makes non-spiking neurons more sensitive to noise than spiking ones (Sarpeshkar, 1998).

Spiking neurons are often perceived as the only information processing component of the nervous system. However, in a large diversity of nervous tissues in both vertebrate and invertebrate species, non-spiking neurons are prominent, such as most of the retina neurons (Field and Chichilnisky, 2007), a majority of *C. elegans* neurons (Goodman et al., 1998), the motorneurons of the *Ascaris* worm (Davis and Stretton, 1989b,a), or many interneurons in insects and crustaceans (Roberts and Bush, 1981). These neurons have been proven to play a paramount role in the functioning of these nervous systems. For instance, depolarizing currents received by non-spiking interneurons can reset biological central pattern generator rythms in insects (Bidaye et al., 2018). Also, they can suppress the appearance of irregular variations of neural activity in small networks of spiking neurons

(Koch et al., 1989). Last, they are central in neuronal integration (Roberts and Bush, 1981) and provide a determining mechanism for the control of motor behaviors (Burrows et al., 1988; Laurent and Burrows, 1989a,b).

Despite their differences in the characteristics of their electrical signals, spiking and non-spiking neurons share similar mechanisms for transmitting them by active and passive propagation. Indeed, both types of neurons exhibit similar ion channels on their membranes, including a large diversity of classical voltage-dependent ion channels which have been experimentally and genetically identified in different non-spiking cell types (Roberts and Bush, 1981; Van Hook et al., 2019). Therefore, to characterize the non-spiking behavior, several works have built conductance-based models (CBMs) of retina neurons (Usui et al., 1996; Liu and Kourennyi, 2004; Publio et al., 2006; Kamiyama et al., 2009) or *C. elegans* neurons (Nicoletti et al., 2019; Naudin et al., 2020, 2022a; Jiménez Laredo et al., 2022) for instance.

CBM is an accurate biophysical representation of the neuron in which every individual parameter and state variable have an established electrophysiological meaning. Therefore, it is broadly used to understand 'low-level' functions of neural systems (Eliasmith and Trujillo, 2014; O'Leary et al., 2015). In particular, it is been extensively used to describe the effect of conductance variations on spiking neuronal dynamics, both at the single-cell (Drion et al., 2015; Berry and Genet, 2021) and at the network levels (Giovannini et al., 2017; Aussel et al., 2018). Such computational works have also been widely employed to study the homeostatic compensatory mechanisms of ion channels in a neuron (Achard and De Schutter, 2006; Soofi et al., 2012; Alonso and Marder, 2019; Onasch and Gjorgjieva, 2020). Indeed, much experimental evidence suggests that a given neuron can maintain a specific electrophysiological signature from different combinations of its individual components, *e.g.* ion channels (Goaillard and Marder, 2021; Kamaleddin, 2021). For instance, experimental measurements have shown two- to six-fold variability in ion channels in the same identified neuron from different crabs (Schulz et al., 2006).

To our knowledge, there is no equivalent computational work that has systematically described the effect of conductance variations on the dynamics of non-spiking neurons, and the possible resulting compensatory effects. Therefore, the aim of this paper is to determine the effect of calcium and potassium conductance (g_{Ca} and g_K) variations on the dynamics of non-spiking neurons, based on experimental observations in the biological literature, and illustrated with a mathematical analysis of a well-posed non-spiking retinal cone model (Kourennyi et al., 2004). Then, we discuss the computational implications on the neuron dynamics of these variations, and we propose a general pattern of the evolution

of non-spiking neuron dynamics (or "phenotypes") as g_{Ca} and g_K evolve. Ion conductance variations could represent possible gain- or loss-of-function mutations in the genes encoding Ca^{2+} and K^+ channel sub-units. Then, we study the possible compensations between I_{Ca} and I_K for which the quantitative behavior and phenotype of the neuron are maintained.

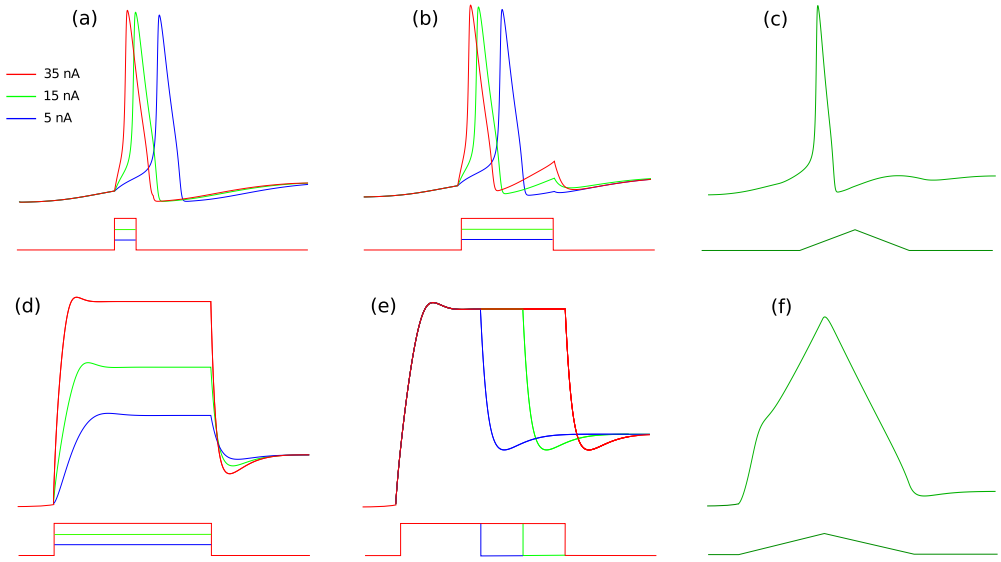

Figure 1: Difference of features between action potentials (a-c) and graded potentials (d-f). Action potentials have been simulated from the classical Hodgkin-Huxley model, while graded potentials have been obtained by reducing its maximal conductances g_{Na} and g_K. The amplitude and waveform of the action potentials are essentially invariant with respect to the (a) amplitude, (b) duration, and (c) waveform of the stimulus, while the amplitude and waveform of the graded potentials are dependent on the (d) amplitude, (e) duration, and (f) waveform of the stimulus. This figure has been reproduced from Naudin et al. (2022a) with the consent of the authors.

2 Results

Phenotypic classification of non-spiking neurons based on the steady-state current shape. Two fundamental behaviors of non-spiking neurons exist: near-linear and bistable. The near-linear behavior is defined by smooth depolarizations or hyperpolarizations from the resting potential, while the bistable one is characterized by nonlinear transitions between the resting potential and a depolarized potential. Among the bistable behaviors, we can distinguish two distinct phenotypes depending on whether the neuron has one or two resting potentials. Therefore, we define three non-spiking neuron phenotypes:

near-linear (phenotype 1), bistable with one resting potential (phenotype 2), and bistable with two resting potentials (phenotype 3). Figure 1. A shows experimental examples of each phenotype.

What confers the neuro-computational characteristics to non-spiking neurons is the steady-state current, noted I_∞ (see Naudin et al. (2022a) or Materials and Methods). As a consequence, these three phenotypes can be distinguished on the basis of their steady-state current shape (Figure 1.B). A monotonic steady-state current confers a phenotype 1 on the neuron. A N-shaped steady-state current with only one zero endows the neuron with a phenotype 2. And a N-shaped steady-state current with two stable zeros gives to the neuron a phenotype 3. In the following paragraphs, we investigate how variations in calcium and potassium conductances are expected to affect the steady-state current, and thus the phenotype, of non-spiking neurons based on experimental observations, and illustrate this using a generic bistable non-spiking CBM.

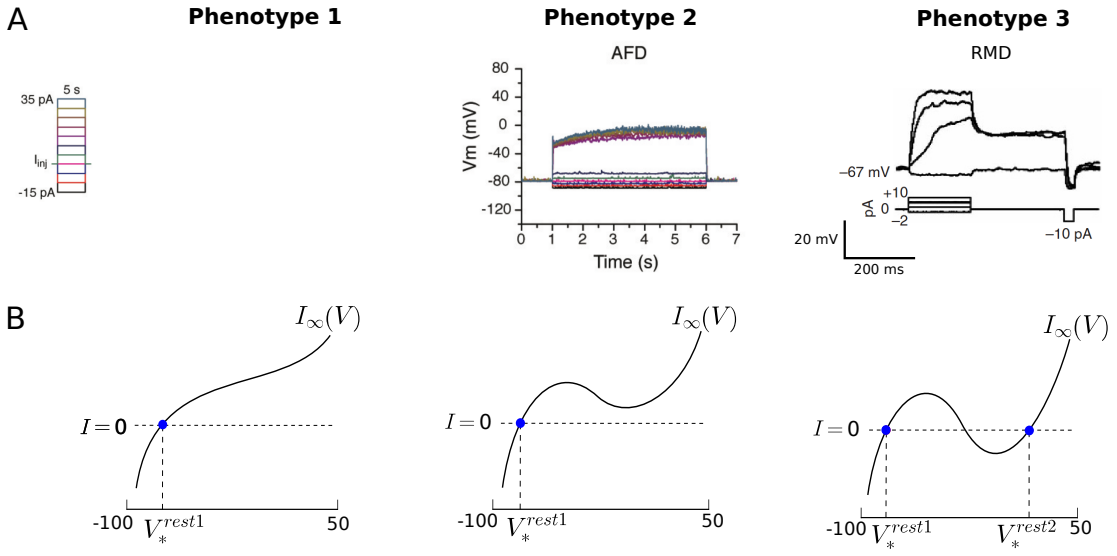

Figure 2: **(A)** Experimental voltage examples from *C. elegans* of each phenotype for a series of current injections starting from −15pA and increasing to 35pA by 5pA increments for the RIM and AFD neurons, and starting from −2pA and increasing to 10pA by 3pA increments for the RMD neuron. The experimental data of the RIM and AFD neurons have been reproduced from Liu et al. (2018), and from Mellem et al. (2008) for the RMD neuron with the consent of the authors. **(B)** Shape of the steady-state current curve associated with each phenotype.

Changes in calcium and potassium conductances drive opposite transitions between neuron phenotypes. In this paper, we use a well-posed retinal cone model (see

Materials and Methods) to illustrate and assess the effect of conductance variations on non-spiking neuronal dynamics. Since the steady-state current determines the qualitative characteristics and the phenotype of a non-spiking neuron, we observe its evolution as g_{Ca} and g_K evolves. It can be seen in Figure 3 that the variations of g_{Ca} and g_K have opposite effects on the evolution of the steady-state current shape of the model. Indeed, the wild-type (WT) steady-state I–V relation (g_{Ca} = 4.92nS and g_K = 2nS) exhibits a region with negative slope that becomes less and less steep and then disappears as g_{Ca} decreases or g_K increases. In other words, the decrease of g_{Ca} leads to the transition from a phenotype 3 to a phenotype 2 and then to a phenotype 1. The same phenotypic changes occur as g_K increases, so that variations in g_{Ca} and g_K have opposite effects. This is consistent with experimental observations on the non-spiking bistable ASER neuron of *C. elegans* for which the negative slope region of its steady-state current is due to the opposition of K^+ and Ca^{2+} currents (Goodman et al., 1998). In addition, these authors show that the voltage-dependence of membrane current is similar in 42 unidentified neurons, suggesting that the ubiquitous flat region of the steady-state current in *C. elegans* neurons share the same common underlying mechanism (opposition of K^+ and Ca^{2+} currents). A similar mechanism is described in vertebrate hair cells in which the flat region of their membrane current-voltage relationship results from a counterbalanced flow of I_K and I_{Ca} (Art and Goodman, 1996; Fettiplace, 1987). Furthermore, in a small group (15%) of thalamocortical neurons, the low threshold T-type Ca^{2+}-current (I_T) is also responsible for an intrinsic bistability (Hughes et al., 1999; Williams et al., 1997). Augmentation of endogenous I_T by an artificial analog transforms all non-bistable thalamocortical neurons to bistable cells (Hughes et al., 1999), which is still consistent with results depicted in Figure 3 (left).

Last, it is worth noting that a new phenotype appears for very large values of g_{Ca} and very small values of g_K. Indeed, for these values, the steady-state current is N-shaped with a negative local maxima. This involves a hyperpolarizing voltage jump (Figure S1), in contrast to phenotype 2 which exhibits a depolarizing jump of the voltage. The shape of the steady-state current is similar to the phenotype 2 (N-shaped with only one zero) so we can name this one the phenotype 2*. However, to our knowledge, this type of non-spiking behavior has never been observed experimentally.

In the following, we describe the computational implications of phenotypic transitions on the neuronal dynamics. As an illustration, we consider the decreasing variations of the calcium conductance g_{Ca}. Therefore, we first describe the computational characteristics of the wild-type neuron phenotype which is phenotype 3, and its phenotype 2 and then 1 resulting from the decrease in g_{Ca} that would reflect calcium channel dysfunctions.

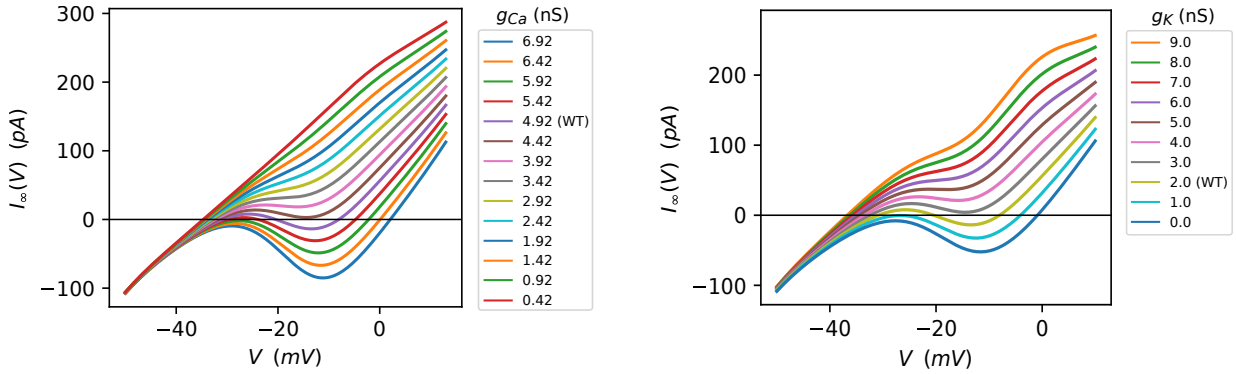

Figure 3: **Evolution of the steady-state current curve as the value of calcium conductance g_{Ca} (left) and potassium conductance g_K (right) vary.**

Computational characteristics of the neuron phenotype 3. The wild-type neuron (g_{Ca} = 4.92nS) displays a N-shaped steady-state current with two stable zeros corresponding to the two values of the resting potential (V_*^{rest1} and V_*^{rest2}) (Figure 4.A). The neuron then has a bistable behavior (Figure 4.B). The existence of the second resting value V_*^{rest2} has an important computational implication: the response of the cell depends on its recent history of activity by storing information about its last input. Figure 4.C illustrates such a phenomenon. The membrane potential of the neuron under 2000ms of a current injection step at 5pA stabilizes at about −29mV. However, if a sufficiently high transient prestimulus is applied, the membrane potential relaxes to its highest resting potential value V_*^{rest2} (approximately −8mV), and finally stabilizes at about −6mV in response to the same current injection protocol as before (current injection step at 5pA under 2000ms). The response of the neuron to a given stimulus then depends on its history of activity. From a dynamical system viewpoint, this is explained by the fact that the shock pulse resets the initial condition of the system at V_*^{rest2} (Izhikevich, 2007). This can be seen in Figure 4.D: if a transient stimulus higher than I_{T2} is applied (for example, I = 20pA), then the new initial condition of the voltage is at V_*^{rest2} after cessation of the current. Therefore, for new hyperpolarization or depolarization inputs higher than $I > I_{T1}$ (for example, I = 5pA), the dynamics of the voltage will converge to the stable equilibrium $V_{2*}^{I_5}$, and not $V_{1*}^{I_5}$, since V_*^{rest2} belongs to the attraction domain of $V_{2*}^{I_5}$. To return to V_*^{rest1}, an injection current lower than I_{T1} has to be applied.

Computational characteristics of the neuron phenotype 2. For a reduced calcium conductance value (for example, g_{Ca} = 4.12nS), the neuron still exhibits a N-shaped steady-state current, but with only one zero (Figure 5.A). The neuron then displays a bistable

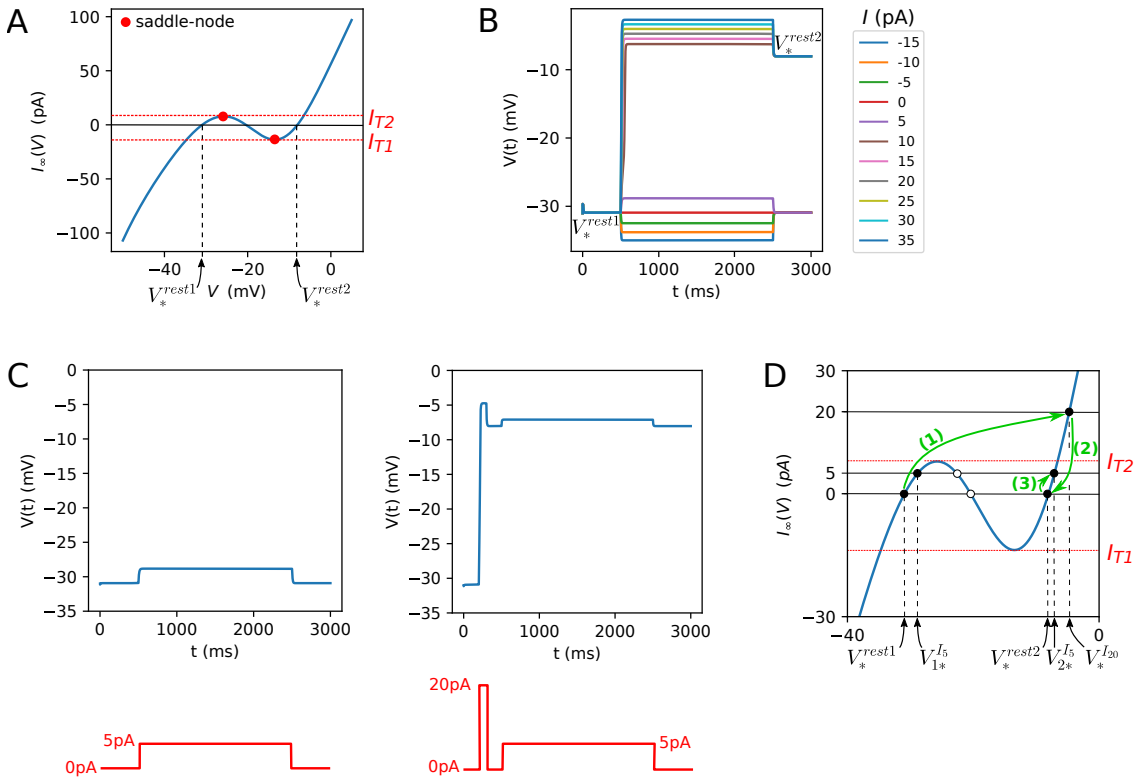

Figure 4: **Features of the wild-type bistable dynamics (phenotype 3). (A)** Wild-type steady-state current displaying a N-shape with two stable zeros corresponding to the two values of the resting potential (V_*^{rest1} and V_*^{rest2}). The saddle points (red dots) correspond to the thresholds of the jump between the two plateau potentials of the bistable neuron, namely for $I_{T1} \approx -13.744$pA and $I_{T2} \approx 7.865$pA. **(B)** Bistable dynamics of the cell voltages for a series of current injections starting from −15pA and increasing to 35pA by 5pA increments. The jump to the upper voltage plateau occurs at I_{T2}. **(C)** Comparison of the voltage dynamics resulting from two different stimulation protocols. (Left) A depolarizing current step (5pA) of 2000ms duration into the neuron is applied. On cessation of the current step, the voltage stabilizes to V_*^{rest1}. (Right) A current pulse (20pA > I_{T2}) of 100ms duration is first injected into the neuron, followed by a step current (5pA) of 2000ms duration. Upon cessation of the current step, the voltage relaxes to its higher resting potential value V_*^{rest2}. **(D)** Diagram explaining (C). (1) A brief transient stimulus (20pA) is applied and the voltage converges to $V_*^{I_{20}}$. (2) The stimulus ceases so that the voltage relaxes to V_*^{rest2} which is the new voltage initial condition. (3) A new depolarizing current step (5pA) is applied and the voltage goes to $V_{2*}^{I_5}$ and not $V_{1*}^{I_5}$ since V_*^{rest2} now belongs to the basin of attraction of $V_{2*}^{I_5}$.

behavior with only one resting potential (V_*^{rest1}) (Figure 5.B). The neuron has lost its short-term memory capacity, so the cell's response no longer reflects the history of its inputs and of its activity (Figure 5.C). The transition from two resting values to a single one is also observed experimentally in the *C. elegans* RMD neuron in mutants for voltage-gated calcium channels (Mellem et al., 2008). Moreover, compared with the wild-type phenotype, we observe that the peak amplitude of the voltages is reduced when g_{Ca} is decreasing (compare Figure 4.B with Figure 5.B), which is still in agreement with experimental data from the *C. elegans* RMD neuron (Mellem et al., 2008). Also, the value of the jump thresholds increases as g_{Ca} decreases (Figure S2), implying a loss of the overall voltage amplitude of the neuron. Indeed, as an example, the peak amplitude in the reduced and the wild-type neuron for I = 10pA is about −29mV and −7mV, respectively.

Computational characteristics of the neuron phenotype 1. When the value of the calcium conductance decreases sufficiently (for example, g_{Ca} = 2.42nS), the steady-state current becomes monotonic (Figure 6.A), which implies the loss of the bistability of the neuron in favor of a near-linear behavior (Figure 6.B). However, it is important to note that the transition from bistable to near-linear voltage behavior is graded, in the sense that the amplitude of the voltage jump decreases in a smooth manner during the transition (Figure S3). The transition from a bistable behavior to a near-linear one is also observed experimentally in the *C. elegans* bistable RMD neuron when extracellular fluid is Ca^{2+}-free (representing approximately the case g_{Ca} = 0nS) (Mellem et al., 2008). The same transition occurs experimentally in the bistable rabbit retinal horizontal cell of phenotype 1: calcium channels blockade results in a near-linear behavior (Aoyama et al., 2000). Finally, the current is less and less sustained as g_{Ca} decreases, making the neuron less and less sensitive to depolarizing inputs (see also Figure S3). This implies that the amplitude of the voltage is decreased when g_{Ca} is reduced.

Following the series of results determined and discussed above, combined with experimental observations from the biological literature, Figure 7 summarizes the evolution of the phenotypic dynamics of non-spiking neurons under the effect of calcium or potassium conductance variations. Experimental observations suggest, however, that these variations may compensate for each other over a certain range of functioning. The objective of the following paragraph is therefore to study these plausible compensations.

Restricted range of ion channel compensations. It is well-known that a given identified neuron can maintain a specific electrophysiological feature from different combinations of its components (*e.g.* ion channels). Indeed, many experimental observations reveal that

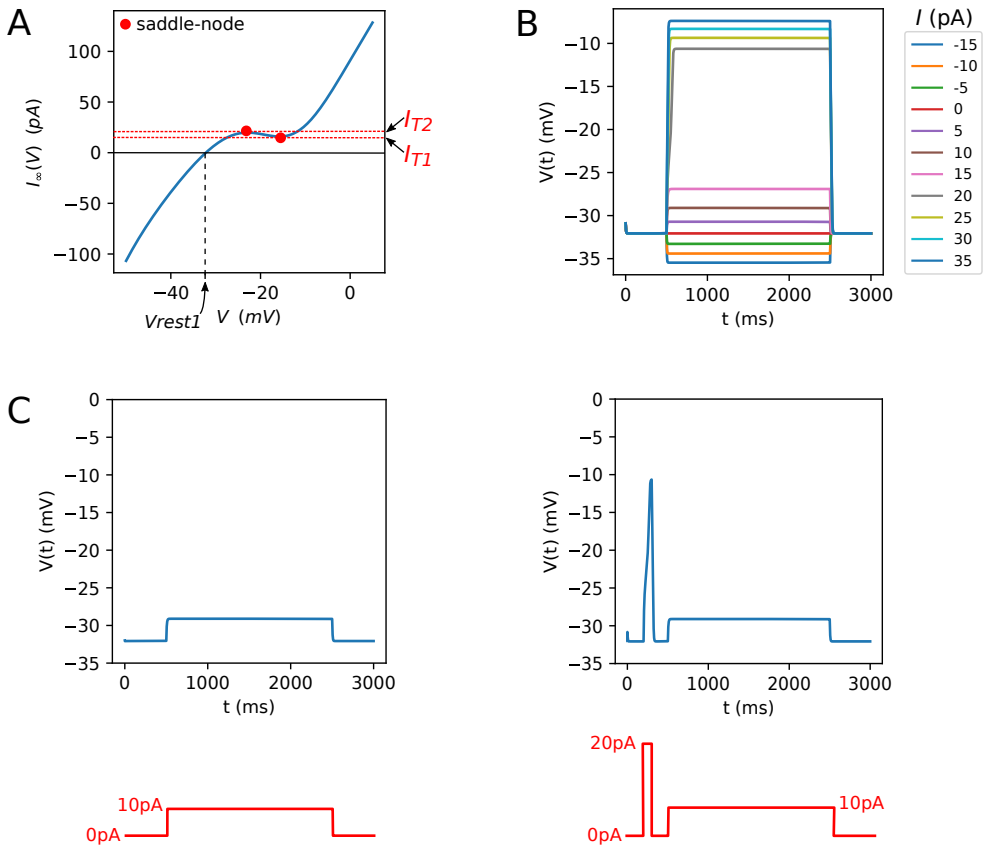

Figure 5: **Features of the bistable dynamics when calcium conductance g_{Ca} is diminished (phenotype 2). (A)** Steady-state current displaying a N-shape with only one zero corresponding to the resting membrane potential of the neuron. The saddle points (red dots) correspond to the thresholds of the jump between the two plateau potentials of the bistable neuron, namely for $I_{T1} \approx 12.275$pA and $I_{T2} \approx 18$pA. **(B)** Bistable dynamics of the neuron voltages for a series of current injections starting from −15pA and increasing to 35pA by 5pA increments. The jump to the upper plateau of voltages occurs at I_{T2}. **(C)** Comparison of the voltage dynamics resulting from two different stimulation protocols described in Figure 4.C. Whatever the stimulation protocol used, the neuron relaxes to a steady-state value of about −29mV: the neuron's response does not reflect the history of its inputs.

a same identified neuron exhibits two to six-fold variability in its ion channels while displaying similar voltage behaviors (Kamaleddin, 2021; Goaillard and Marder, 2021). Here we explore and study these possible compensatory mechanisms between I_{Ca} and I_K in the non-spiking CBM under study, from a qualitative and quantitative viewpoint.

It can be observed in Figure 8.A that each neuron phenotype of the model exists

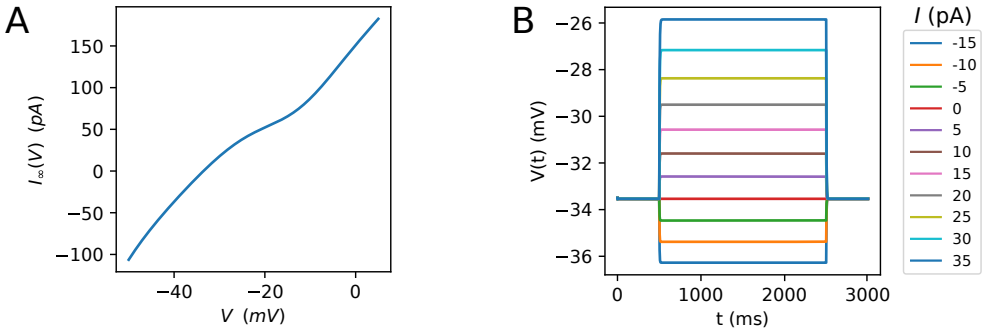

Figure 6: **Features of the neuron dynamics when calcium conductance g_{Ca} is highly reduced (phenotype 1). (A)** Steady-state current of the neuron, that exhibits a monotonic shape unlike the wild-type neuron that has a N-shape. **(B)** Resulting near-linear behavior of the neuron.

within a certain range of g_{Ca} and g_K values. As explained above, the transition between phenotype 2 and phenotype 1 is graded in the sense that the amplitude of the voltage jump decreases in a smooth manner during the transition from bistable to near-linear behavior. Conversely, the transition between phenotype 2* and phenotype 3, and between phenotype 3 and phenotype 2, occurs abruptly and immediately. The vertical dashed line indicates the value of g_{Ca} ($\simeq 3.40$nS) at which g_K can no longer compensate for the decrease in g_{Ca} to preserve the wild-type phenotype. Indeed, for $g_{Ca} \simeq 3.40$nS, g_K is equal to 0 and therefore can no longer decrease to compensate for the decrease in g_{Ca}. The neuron then switches to phenotype 2. On the contrary, for every decreased g_K value, there are compensating decreasing g_{Ca} values for which the wild-type phenotype is maintained. We can therefore suggest that g_{Ca} variations (*i.e.* possible loss-of-functions of calcium channels) are more difficult for the system to compensate than g_K variations (*i.e.* possible loss-of-functions of potassium channels). However, in vivo, this interpretation would depend of physiologically plausible values of g_K and g_{Ca}.

Furthermore, we determine a quantitative relationship between g_{Ca} and g_K (see Materials and Methods) that yield similar behaviors of the model voltages (Figure 8.B). More specifically, we find an affine relationship between g_{Ca} and g_K given by

$$g_K = 1.6517 g_{Ca} - 6.114. \tag{1}$$

Some examples of the different solutions obtained from this relation are shown in Figure 8.C. However, it can be noted that the more g_{Ca} decreases, the more g_K must decrease to compensate, and the less accurately it compensates (Figure S4). Such a characteristic can also be seen in Figure 8.C ($g_{Ca} = 3.72$nS, $g_K = 0.02$nS) on which it appears that the

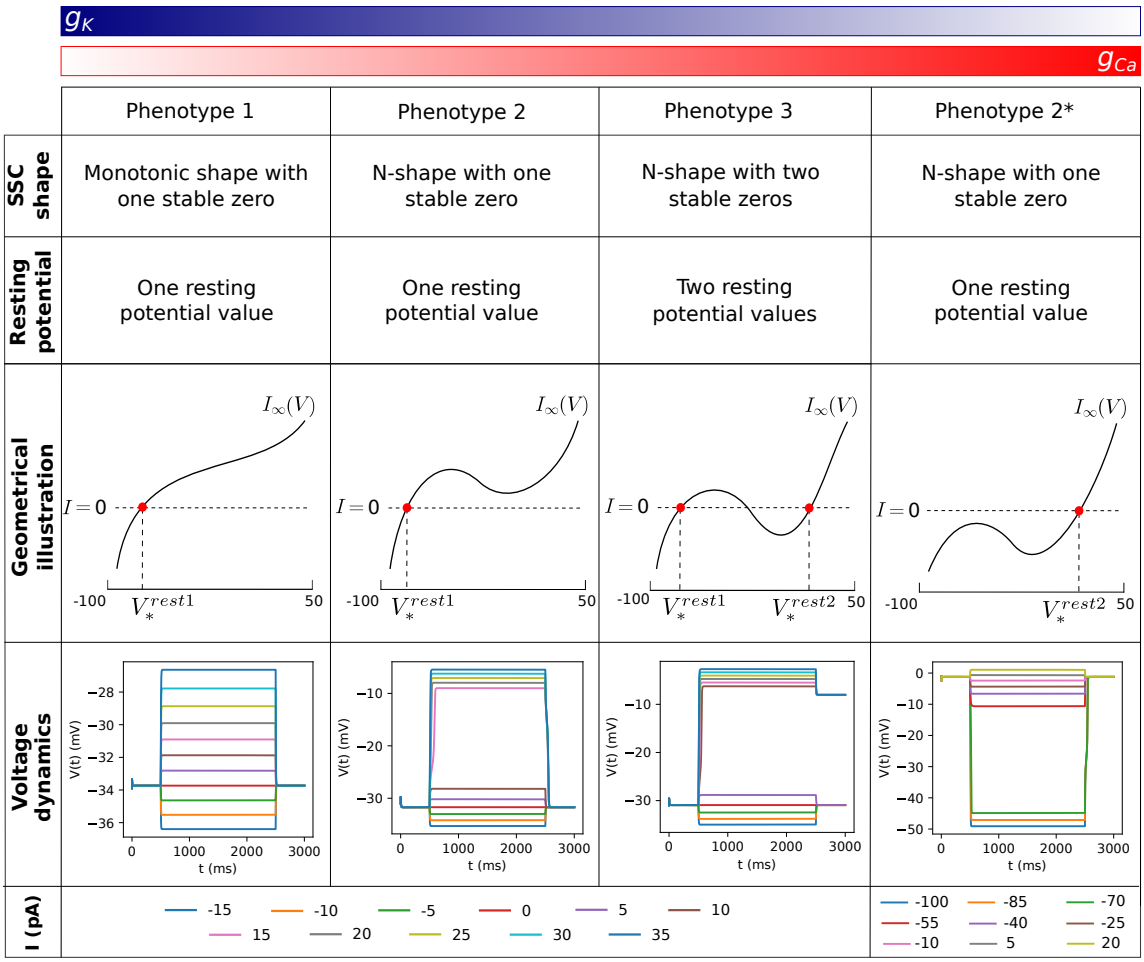

Figure 7: **General pattern of the effect of changes in calcium and potassium conductances on the non-spiking neuron dynamics.** There are three physiological behaviors of non-spiking neurons (phenotype 1, 2 and 3), while phenotype 2* has never been observed experimentally. Variations in calcium and potassium conductances drive opposite transitions between these neuron phenotypes, involving a modification of the computational characteristics of the neuron. As an illustration, we took a well-posed retinal cone model, with a wild-type phenotype 3. Such a neuron displays two resting potential values corresponding to the intersections between the curve I_∞ and the horizontal line $I = 0$. The neuron is endowed with a short-term memory capacity, that is, the response of the cell depends on its recent history of activity by storing information about its last inputs. The decrease of g_{Ca} implies a unique intersection between I_∞ and the horizontal line $I = 0$: the bistable neuron then has only one resting potential (phenotype 2), which implies the loss of its short-term memory capacity. Finally, the decrease of g_{Ca} leads to the loss of the bistability of the neuron: it becomes near-linear (phenotype 1).

voltage jump occurs for relatively higher values of injection currents.

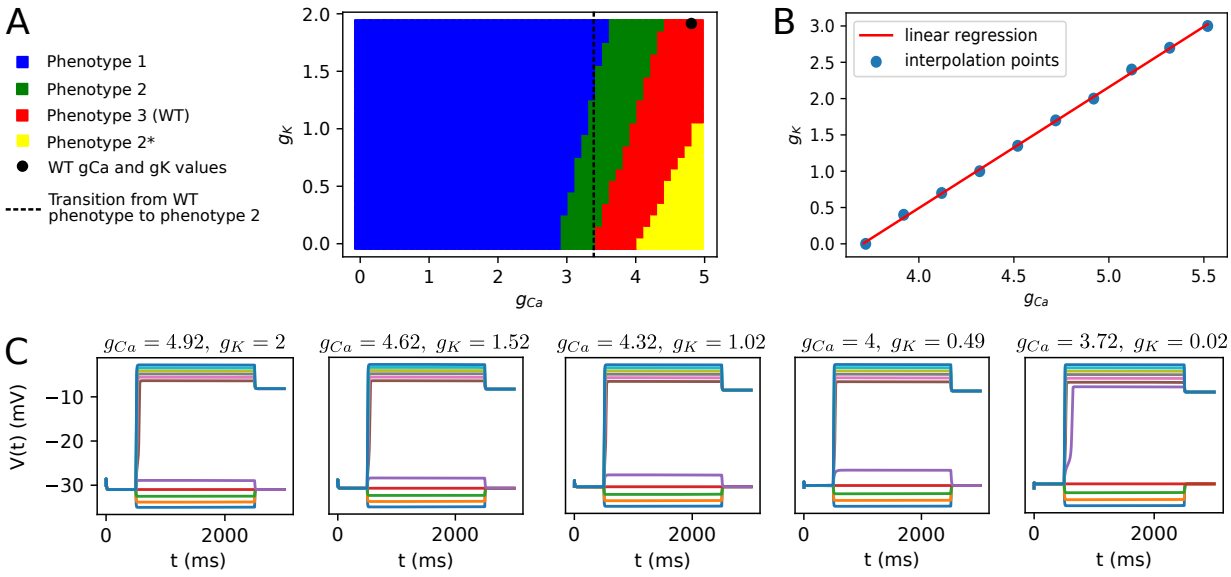

Figure 8: **(A)** Parameter landscape of neuron phenotypes as a function of g_{Ca} and g_K. **(B)** Quantitative affine relationship between g_{Ca} and g_K that gives similar voltage behaviors. **(C)** Example of similar voltage behaviors obtained from the relationship determined in (B), for a series of current injections starting from −15pA and increasing to 35pA by 5pA increments.

3 Discussion

Non-spiking neurons are ubiquitous in many neuronal processes and are found in a wide variety of nervous tissues, whose the *C. elegans* and retinal networks are important examples. Based on the literature in experimental biology and on mathematical analyses we performed, three distinct phenotypes of non-spiking neurons were determined depending on the shape of their steady-state current. A phenotype 3 neuron is bistable with two resting potentials (N-shaped steady-state current with two stable zeros), a phenotype 2 neuron is also bistable but with only one resting potential (N-shaped steady-state current with one zero), while a phenotype 1 neuron is near-linear (monotonic steady-state current). A fourth phenotype was highlighted from the mathematical analysis of a well-posed retinal cone model. Such a phenotype is characterized by a N-shaped steady-state current with one zero and a negative local maxima, resulting in a hyperpolarizing voltage jump. However, to our knowledge, this non-spiking phenotype has never been observed experimentally.

Then, we showed that changes in calcium and potassium conductances (g_{Ca} and g_K)

drove opposite transitions between neuron phenotypes. A general pattern of the evolution of non-spiking neuron dynamics as g_{Ca} and g_K evolves was then determined, and the computational implications on the neuron dynamics were discussed. In particular, we showed that a neuron with a phenotype 3 could switch to a phenotype 2 and then 1 as g_{Ca} decreases or g_K increases. In other words, the neuron first lost its short-term memory capacity (transition from phenotype 3 to 2), then lost its bistable behavior to a near-linear one (transition from phenotype 2 to 1).

Finally, we studied the homeostatic compensatory mechanisms between I_{Ca} and I_K in the retinal cone model. In particular, we showed that there is a restricted range of ion conductance values g_{Ca} and g_K for which the phenotype and the behavior of the model are maintained. Further, we highlighted that variations in g_{Ca} are more difficult for the system to compensate than variations in g_K.

Phenotypic classification and intra-phenotype diversity. In this paper, we propose a classification of non-spiking neurons based on qualitative arguments derived from mathematical considerations. Specifically, as the steady-state current determines the qualitative characteristics of non-spiking neurons, the classification is based on its shape. Based on a state-of-the-art research in biology, Table 1 inventories for each phenotype class a series of experimentally identified neurons from different nervous tissues. However, it is worth noting that there are quantitative differences in behavior between neurons in each class, so that an intra-phenotype diversity exists. Indeed, as a representative example, we can compare the RIM and AIY neurons from *C. elegans* that are both of phenotype 1 (Figure S5). While AIY is more sensitive to hyperpolarizing than depolarizing inputs with a transition point around −30mV, RIM is depolarized or hyperpolarized in a smooth manner due to the lack of large sustained currents. The steady-state current of these neurons characterizes and reveals its differences (Naudin et al., 2022b), so that the addition of subclasses to differentiate qualitative features between neurons of the same class could still be done based on the steady-state current shape.

Implications of phenotypic changes on retinal visual information processing. The retina is a sensory organ located on the inner surface of the eye whose role is mainly to receive light stimuli and perform a primary visual information processing, the phototransduction. The light is captured and converted in electrical signals by the photoreceptor cells (cones and rods), then conveyed through several relays (horizontal, bipolar and amacrine cells) before reaching the ganglion cells, the last relay of phototransduction. All the retinal neurons are non-spiking except the ganglion cells, which trigger spikes. Visual information,

	Phenotype 1	Phenotype 2	Phenotype 3
Retina	Rod (Mao et al., 2003; Kamiyama et al., 2009) Amacrine (Boos et al., 1993)	Bipolar (Usui et al., 1996; Mao et al., 2003; Schilardi and Kleinlogel, 2021)	Cone (Kourennyi et al., 2004; Ko et al., 2007) Horizontal (Aoyama et al., 2000)
C. elegans	RIM (Liu et al., 2018) AVA (Mellem et al., 2008) VA5 (Liu and Kourennyi, 2004) PLM (O'Hagan et al., 2005) AVE (Lindsay et al., 2011) AIY (Liu et al., 2018) VB6 (Liu et al., 2017) DVC (Jiang et al., 2022) RIS (Jiang et al., 2022) Many non identified neurons (Goodman et al., 1998)	ASER (Goodman et al., 1998) AWC (Ramot et al., 2008) ASH (Geffeney et al., 2011) AFD (Liu et al., 2018) AIA (Dobosiewicz et al., 2019) Many non identified neurons (Goodman et al., 1998)	RMD (Mellem et al., 2008) Many non identified neurons (Goodman et al., 1998)
Ascaris	Motorneurons (Davis and Stretton, 1989a)		

Table 1: Classification of non-spiking neurons following three phenotypes. Phenotype 1 comprises near-linear neuron. Phenotype 2 bistable neurons with only one resting potential. Phenotype 3 bistable neurons with two resting potentials.

encoded by the spikes of ganglion cells, is then transmitted over long distances via the optic nerve formed by the axons of these cells to higher visual brain centers.

The electrical signal that propagates through each population of retinal cells is underpinned by the existence of various calcium and potassium channels revealed by electrophysiological studies (Van Hook et al., 2019). Mutations in genes encoding for these ion

channels have been shown to be ubiquitous in retinal cells in various disorders (Heyes et al., 2015; Waldner et al., 2018; Kilicarslan et al., 2021; Mayama, 2014). The results obtained in this paper suggest that such modifications in retinal cell ion channels could affect the integrity of the transmitted signal through phenotypic changes. How such changes in the retinal non-spiking neurons ultimately affect the ganglion cell output is then a question of interest, and will require further modeling studies that we are currently conducting.

4 Materials and methods

Conductance-based models (CBMs). In CBMs, the dynamics of the membrane potential V is described by a general equation of the form

$$C\frac{\mathrm{d}V}{\mathrm{d}t} = -\sum_{ion} I_{ion} + I \tag{2}$$

where C is the membrane capacitance, $\sum_{ion} I_{ion}$ is the total current flowing accross the cell membrane, and I is an applied current. The currents I_{ion} take the form

$$I_{ion} = g_{ion} m_{ion}^{a} h_{ion}^{b} (V - E_{ion})$$

where m (*resp.* h) denotes the probability for an activation (*resp.* inactivation) gate to be in the open state; a and b are the number of activation and inactivation gates, respectively; g_{ion} is the maximal conductance associated with ion (namely the conductance of the ion channel when all the gates are open); and E_{ion} is the reversal potential,that is, the potential at which the ion current reverses its direction.

Conductance-based model of the retinal cone cell. The conductance-based model of the canonical retinal cone cell is based on the model developed in Kourennyi et al. (2004). It has four ion currents: a calcium current (I_{Ca}), a hyperpolarization activated current (I_h), a delayed rectifying potassium current (I_K), and a leak current (I_L). The parameters are expressed in the following units: mV (voltage), pA (current), nS (conductance), and ms (time). The membrane capacitance (C) is set to 16nF. Leak current is classically described as $I_L = g_L(V - E_L)$ and the remaining currents are described in Table 2.

Bifurcation dynamics of non-spiking CBMs. In non-spiking CBMs, the steady-state current curve I_∞ determines the number of equilibria of the system and their values, as well as the bifurcations of the resting state along with the values to which they occur. It takes the general form

$$I_\infty(V) = \sum_{ion} I_{ion\infty}(V) \quad \text{where} \quad I_{ion\infty}(V) = g_{ion} m_{ion\infty}^{a}(V) h_{ion\infty}^{b}(V)(V - E_{ion}) \tag{3}$$

with

Ion current (I_{ion})	$\alpha_{ion}(V)$ and $\beta_{ion}(V)$ rates	g_{ion} and E_{ion}
$I_{Ca} = g_{Ca} m_{Ca} h_{Ca} (V - E_{Ca})$	$\alpha_{Ca}(V) = 3.1\, e^{(V+16.6)/11.4}$	$g_{Ca} = 4.92$
$\frac{dm_{Ca}}{dt} = \alpha_{Ca}(1 - m_{Ca}) - \beta_{Ca} m_{Ca}$	$\beta_{Ca}(V) = 3.1\, e^{(-V-16.6)/11.4}$	$E_{Ca} = 40$
$I_h = g_h (1 - (1 + 3m_h)(1 - m_h)^3)(V - E_h)$	$\alpha_{m_h}(V) = \frac{18}{(1 + e^{(V+88)/12})}$	$g_h = 3.5$
$\frac{dm_h}{dt} = \alpha_{m_h}(1 - m_h) - \beta_{m_h} m_h$	$\beta_{m_h}(V) = \frac{18}{(1 + e^{-(V+18)/19})}$	$E_h = -32.5$
$I_{Kv} = g_{Kv} m_{Kv}^3 h_{Kv} (V - E_K)$	$\alpha_{m_{Kv}}(V) = \frac{5(V - 100)}{(1 - e^{-(V-100)/42})}$	$g_{Kv} = 2$
$\frac{dm_{Kv}}{dt} = \alpha_{m_{Kv}}(1 - m_{Kv}) - \beta_{m_{Kv}} m_{Kv}$	$\beta_{m_{Kv}}(V) = 9\, e^{(20-V)/40}$	$E_{Kv} = -80$
$\frac{dh_{Kv}}{dt} = \alpha_{h_{Kv}}(1 - h_{Kv}) - \beta_{h_{Kv}} h_{Kv}$	$\alpha_{h_{Kv}}(V) = 0.15\, e^{-V/22}$	
	$\beta_{h_{Kv}}(V) = \frac{0.4125}{(1 + e^{(10-V)/7})}$	

Table 2: Summary of ion currents composing the canonical cone model.

$$x_\infty(V) = \frac{1}{1 + \exp\left(\frac{V_{1/2}^x - V}{k_x}\right)}, \quad x \in \{m, h\}.$$

where $V_{1/2}^x$ and k_x are constant parameters.

Any stationary point of gating variables $x \in \{m, h\}$ must satisfy $x_* = x_\infty(V_*)$. Replacing this into the first equation on V, fixed points V_* of such models satisfy the equation

$$I_\infty(V_*) = I. \tag{4}$$

In other words, equilibria V_* correspond to the intersections between the steady-state curve I_∞ and a horizontal line $I = c$ where c is a constant. There are two standard steady-state curves I_∞, monotonic and cubic (Figure 9), each involving fundamentally different neuro-computational properties for non-spiking neurons:

- As shown in Figure 9.A, CBMs with a monotonic steady-state current only have one equilibrium for any value of I. Non-spiking neurons with such a steady-state current display a near-linear behavior characterized by smooth depolarizations or hyperpolarizations from the resting potential, such as the RIM and AIY neurons (Figure 1.B, left).

- As shown in Figure 9.B, a N-shaped curve leads to a saddle-node bifurcation. When

$I = c_1$, there are 3 equilibria, noted $V_{1*}^{c_1}$, $V_{2*}^{c_1}$ and $V_{3*}^{c_1}$. Increasing I results in coalescence of two equilibria (the stable $V_{1*}^{c_1}$ with the unstable $V_{2*}^{c_1}$). The value $I = c_2$, at which the equilibria coalesce, is called the *bifurcation value*. For this value of I, there exist 2 equilibria. For $I > c_2$, the system has only one equilibrium (*e.g.* $I = c_3$). In summary, when the parameter I increases, a stable and an unstable equilibrium approach, coalesce, and then annihilate each other. Non-spiking neurons with a N-shaped steady-state current display a bistable behavior characterized by a voltage jump between the resting potential and a depolarized potential of higher voltage, such as the AFD neuron (Figure 1.B, right).

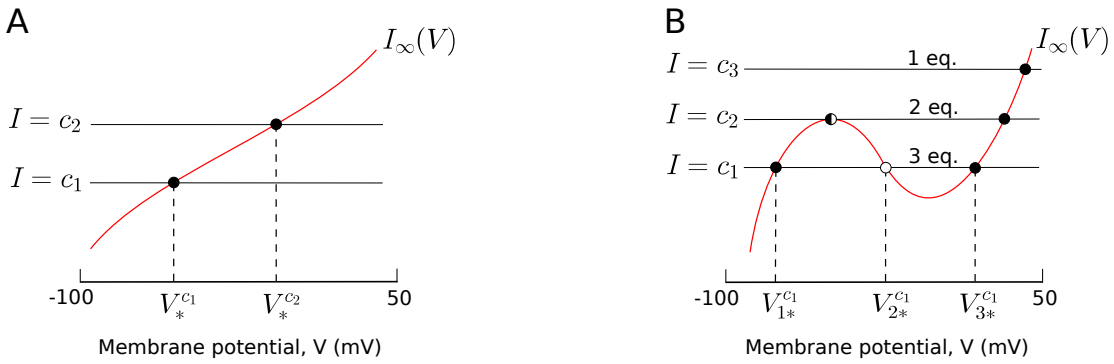

Figure 9: **Two typical shapes of the steady-state current $V \to I_\infty(V)$, in red.** Intersections of I_∞ and horizontal line $I = c$ (with c constant) correspond to equilibria of the system. We denote stable equilibria as filled circles ●, unstable equilibria as open circles ○ and saddle-node equilibria as ◐. **(A)** Monotonic steady-state current. $V_*^{c_1}$ and $V_*^{c_2}$ correspond to equilibria for a current injection $I = c_1$ and $I = c_2$ respectively. **(B)** N-shaped steady-state current. The number of equilibria of the system depends on the value of I. For the sake of readibility, we highlight equilibria only for $I = c_1$, noted $V_{1*}^{c_1}$, $V_{2*}^{c_1}$ and $V_{3*}^{c_1}$.

Therefore, it can be stated that the steady-state current determines the bifurcation structure of non-spiking neurons and the equilibrium values of their graded responses to particular stimuli.

Procedure to build a quantitative relationship between g_{Ca} and g_K. As explained above, the steady-state current determines the neuro-computational features of non-spiking neurons. Therefore, the adjustments of g_{Ca} and g_K to maintain the same neuron behavior are carried out to preserve the wild-type steady-state current. The wild-type conductance value of g_{Ca} is 4.92nS. For a series of decreased and increased values of g_{Ca}, we straightforwardly find a corresponding value of g_K for which we are as close as possible to the

wild-type steady-state current. Then, we perform a linear regression using Python and specific modules.

Acknowledgements

We thank Dr. Mellem and Dr. Liu for their consents to reproduce their experimental data.

Code accessibility

The code used in this paper is available at https://gitlab.com/lois76/conductance_nonspikingneurons_code.

Declaration of competing interests

The authors declare no competing interests.

Supplementary figures

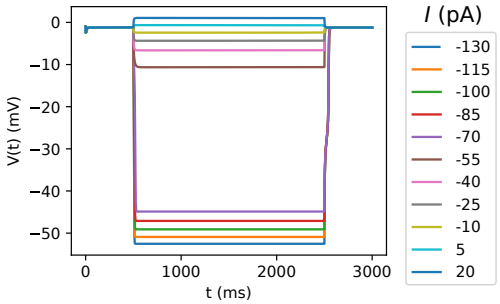

Figure S1: Example of voltage dynamics of phenotype 2*. This phenotype is characterized by a hyperpolarizing jump of the voltage.

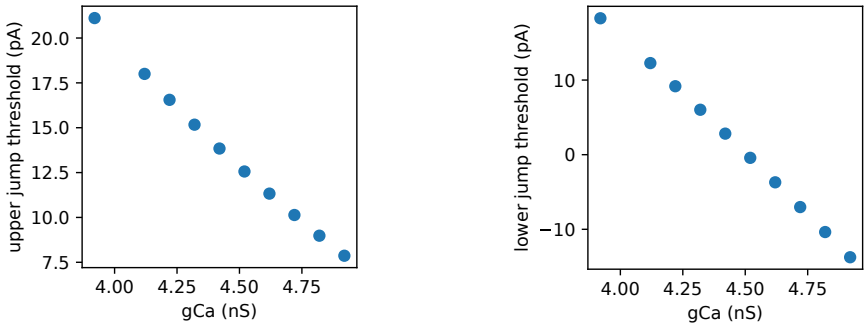

Figure S2: Calcium conductance g_{Ca} against the upper and lower jump thresholds.

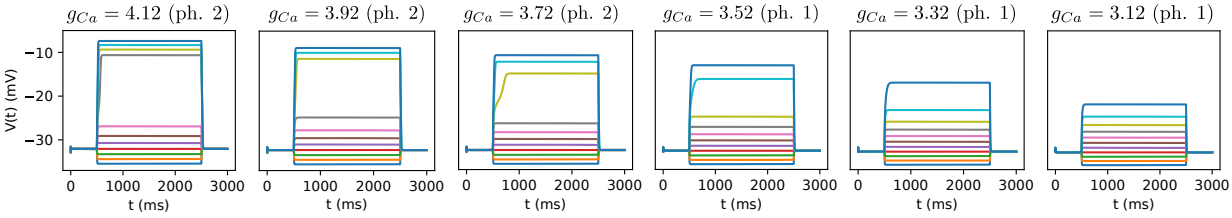

Figure S3: Evolution of the model membrane potentials for a series of current injections starting from −15pA, and increasing to 35pA by 5pA increments, for- different values of g_{Ca}. The transition between the phenotype (ph.) 2 and 1 is graded in the sense that the amplitude of the voltage jump decreases in a smooth manner.

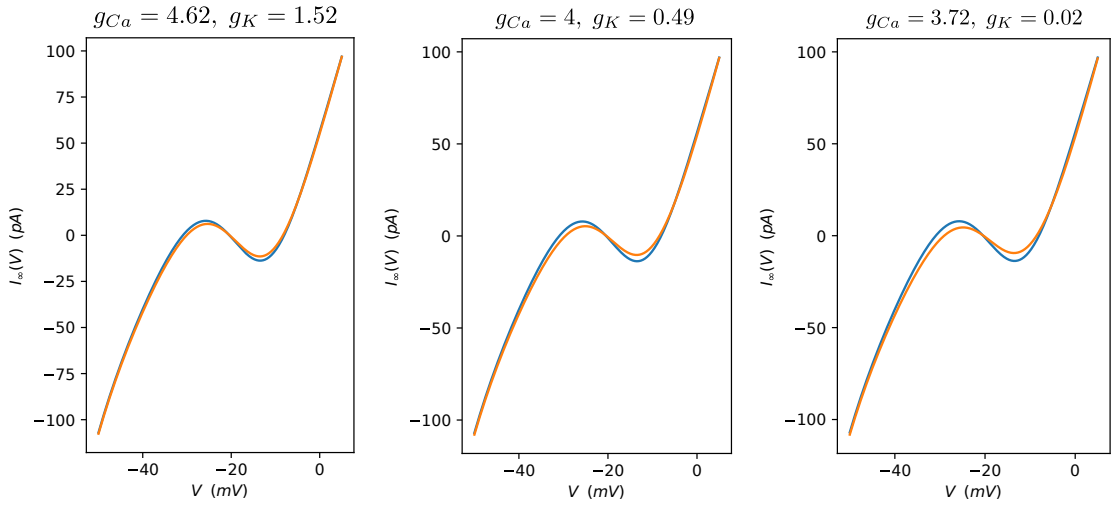

Figure S4: Wild-type steady-state current (in blue), *i.e.* g_{Ca} = 4.92nS and g_K = 2nS, against degenerate steady-state current (in orange) obtained from the equation (1) for different optimal compensatory values of g_{Ca} and g_K.

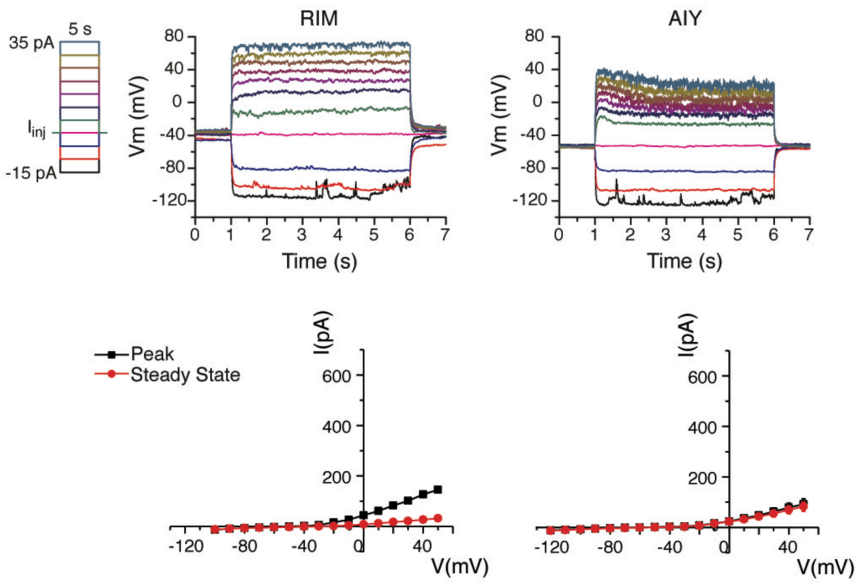

Figure S5: **(Top)** Example of the evolution of membrane potential of phenotype 1 for a series of current injections, in the space of 5 seconds, starting from −15 pA and increasing to 35 pA by 5 pA increments. RIM is depolarized or hyperpolarized in a smooth manner due to the lack of large sustained currents, while AIY is more sensitive to hyperpolarization than depolarization inputs with a transition point around −30mV. **(Bottom)** I-V relationships obtained from averaged voltage-clamp recordings (RIM: n = 3; AIY: n = 7; AFD: n = 3). Peak currents are measured by the absolute maximum amplitude of currents within the first 100 ms of each voltage step onset, while steady-state currents are measured by the averaged currents of the last 50 ms of each voltage step. The experimental data have been reproduced from Liu et al. (2018) with the consent of the authors.

References

P. Achard and E. De Schutter. Complex parameter landscape for a complex neuron model. *PLoS computational biology*, 2(7):e94, 2006.

L. M. Alonso and E. Marder. Visualization of currents in neural models with similar behavior and different conductance densities. *Elife*, 8:e42722, 2019.

T. Aoyama, Y. Kamiyama, S. Usui, R. Blanco, C. F. Vaquero, and P. de la Villa. Ionic current model of rabbit retinal horizontal cell. *Neuroscience Research*, 37(2):141–151, 2000.

J. Art and M. Goodman. Ionic conductances and hair cell tuning in the turtle cochlea a. *Annals of the New York Academy of Sciences*, 781(1):103–122, 1996.

A. Aussel, L. Buhry, L. Tyvaert, and R. Ranta. A detailed anatomical and mathematical model of the hippocampal formation for the generation of sharp-wave ripples and theta-nested gamma oscillations. *Journal of computational neuroscience*, 45(3):207–221, 2018.

H. Berry and S. Genet. A model of on/off transitions in neurons of the deep cerebellar nuclei: deciphering the underlying ionic mechanisms. *The Journal of Mathematical Neuroscience*, 11(1):1–34, 2021.

S. S. Bidaye, T. Bockemühl, and A. Büschges. Six-legged walking in insects: how cpgs, peripheral feedback, and descending signals generate coordinated and adaptive motor rhythms. *Journal of neurophysiology*, 119(2):459–475, 2018.

R. Boos, H. Schneider, and H. Wassle. Voltage-and transmitter-gated currents of all-amacrine cells in a slice preparation of the rat retina. *Journal of Neuroscience*, 13(7): 2874–2888, 1993.

M. Burrows, G. Laurent, and L. Field. Proprioceptive inputs to nonspiking local interneurons contribute to local reflexes of a locust hindleg. *Journal of Neuroscience*, 8(8): 3085–3093, 1988.

M. Czeredys. Dysregulation of neuronal calcium signaling via store-operated channels in huntington's disease. *Frontiers in Cell and Developmental Biology*, 8:1645, 2020.

R. Davis and A. Stretton. Passive membrane properties of motorneurons and their role in long-distance signaling in the nematode ascaris. *Journal of Neuroscience*, 9(2):403–414, 1989a.

R. E. Davis and A. Stretton. Signaling properties of ascaris motorneurons: graded active responses, graded synaptic transmission, and tonic transmitter release. *Journal of Neuroscience*, 9(2):415–425, 1989b.

M. Dobosiewicz, Q. Liu, and C. I. Bargmann. Reliability of an interneuron response depends on an integrated sensory state. *Elife*, 8:e50566, 2019.

G. Drion, T. O'Leary, and E. Marder. Ion channel degeneracy enables robust and tunable neuronal firing rates. *Proceedings of the National Academy of Sciences*, 112(38):E5361–E5370, 2015.

C. Eliasmith and O. Trujillo. The use and abuse of large-scale brain models. *Current opinion in neurobiology*, 25:1–6, 2014.

R. Fettiplace. Electrical tuning of hair cells in the inner ear. *Trends in Neurosciences*, 10 (10):421–425, 1987.

G. D. Field and E. Chichilnisky. Information processing in the primate retina: circuitry and coding. *Annu. Rev. Neurosci.*, 30:1–30, 2007.

S. L. Geffeney, J. G. Cueva, D. A. Glauser, J. C. Doll, T. H.-C. Lee, M. Montoya, S. Karania, A. M. Garakani, B. L. Pruitt, and M. B. Goodman. Deg/enac but not trp channels are the major mechanoelectrical transduction channels in a c. elegans nociceptor. *Neuron*, 71(5):845–857, 2011.

F. Giovannini, B. Knauer, M. Yoshida, and L. Buhry. The can-in network: A biologically inspired model for self-sustained theta oscillations and memory maintenance in the hippocampus. *Hippocampus*, 27(4):450–463, 2017.

J.-M. Goaillard and E. Marder. Ion channel degeneracy, variability, and covariation in neuron and circuit resilience. *Annual review of neuroscience*, 44, 2021.

M. B. Goodman, D. H. Hall, L. Avery, and S. R. Lockery. Active currents regulate sensitivity and dynamic range in c. elegans neurons. *Neuron*, 20(4):763–772, 1998.

S. Heyes, W. S. Pratt, E. Rees, S. Dahimene, L. Ferron, M. J. Owen, and A. C. Dolphin. Genetic disruption of voltage-gated calcium channels in psychiatric and neurological disorders. *Progress in neurobiology*, 134:36–54, 2015.

S. W. Hughes, D. W. Cope, T. I. Tóth, S. R. Williams, and V. Crunelli. All thalamocortical neurones possess a t-type ca2+ 'window' current that enables the expression of bistability-mediated activities. *The Journal of physiology*, 517(3):805–815, 1999.

M. J. Hurley and D. T. Dexter. Voltage-gated calcium channels and parkinson's disease. *Pharmacology & therapeutics*, 133(3):324–333, 2012.

E. M. Izhikevich. *Dynamical systems in neuroscience*. MIT press, 2007.

J. Jiang, Y. Su, R. Zhang, H. Li, L. Tao, and Q. Liu. C. elegans enteric motor neurons fire synchronized action potentials underlying the defecation motor program. *Nature communications*, 13(1):1–15, 2022.

J. L. Jiménez Laredo, L. Naudin, N. Corson, and C. M. Fernandes. A methodology for determining ion channels from membrane potential neuronal recordings. In *Applications of Evolutionary Computation*, pages 15–29. Springer International Publishing, 2022.

M. A. Kamaleddin. Degeneracy in the nervous system: from neuronal excitability to neural coding. *BioEssays*, page 2100148, 2021.

Y. Kamiyama, S. M. Wu, and S. Usui. Simulation analysis of bandpass filtering properties of a rod photoreceptor network. *Vision research*, 49(9):970–978, 2009.

I. Kilicarslan, L. Zanetti, E. Novelli, C. Schwarzer, E. Strettoi, and A. Koschak. Knockout of cav1. 3 l-type calcium channels in a mouse model of retinitis pigmentosa. *Scientific Reports*, 11(1):1–12, 2021.

M. L. Ko, Y. Liu, S. E. Dryer, and G. Y.-P. Ko. The expression of l-type voltage-gated calcium channels in retinal photoreceptors is under circadian control. *Journal of neurochemistry*, 103(2):784–792, 2007.

U. Koch, U. Bässler, and M. Brunner. Non-spiking neurons supress fluctuations in small networks. *Biological cybernetics*, 62(1):75–81, 1989.

D. E. Kourennyi, X.-d. Liu, J. Hart, F. Mahmud, W. H. Baldridge, and S. Barnes. Reciprocal modulation of calcium dynamics at rod and cone photoreceptor synapses by nitric oxide. *Journal of neurophysiology*, 92(1):477–483, 2004.

G. Laurent and M. Burrows. Distribution of intersegmental inputs to nonspiking local interneurons and motor neurons in the locust. *Journal of Neuroscience*, 9(9):3019–3029, 1989a.

G. Laurent and M. Burrows. Intersegmental interneurons can control the gain of reflexes in adjacent segments of the locust by their action on nonspiking local interneurons. *Journal of Neuroscience*, 9(9):3030–3039, 1989b.

T. H. Lindsay, T. R. Thiele, and S. R. Lockery. Optogenetic analysis of synaptic transmission in the central nervous system of the nematode caenorhabditis elegans. *Nature communications*, 2(1):1–9, 2011.

P. Liu, B. Chen, R. Mailler, and Z.-W. Wang. Antidromic-rectifying gap junctions amplify chemical transmission at functionally mixed electrical-chemical synapses. *Nature communications*, 8(1):1–16, 2017.

Q. Liu, P. B. Kidd, M. Dobosiewicz, and C. I. Bargmann. C. elegans awa olfactory neurons fire calcium-mediated all-or-none action potentials. *Cell*, 175(1):57–70, 2018.

X.-D. Liu and D. E. Kourennyi. Effects of tetraethylammonium on kx channels and simulated light response in rod photoreceptorss. *Annals of biomedical engineering*, 32(10): 1428–1442, 2004.

S. R. Lockery, M. B. Goodman, and S. Faumont. First report of action potentials in a c. elegans neuron is premature. *Nature neuroscience*, 12(4):365–366, 2009.

B.-Q. Mao, P. R. MacLeish, and J. D. Victor. Role of hyperpolarization-activated currents for the intrinsic dynamics of isolated retinal neurons. *Biophysical journal*, 84(4):2756–2767, 2003.

C. Mayama. Calcium channels and their blockers in intraocular pressure and glaucoma. *European Journal of Pharmacology*, 739:96–105, 2014.

J. E. Mellem, P. J. Brockie, D. M. Madsen, and A. V. Maricq. Action potentials contribute to neuronal signaling in c. elegans. *Nature neuroscience*, 11(8):865–867, 2008.

L. Naudin, N. Corson, M. Aziz-Alaoui, J. L. J. Laredo, and T. Démare. On the modeling of the three types of non-spiking neurons of the caenorhabditis elegans. *International Journal of Neural Systems*, page S012906572050063X, 2020.

L. Naudin, J. L. Jiménez Laredo, Q. Liu, and N. Corson. Systematic generation of biophysically detailed models with generalization capability for non-spiking neurons. *PloS one*, 17(5):e0268380, 2022a.

L. Naudin, J. L. J. Laredo, and N. Corson. A simple model of non-spiking neurons. *hal*, 2022b.

M. Nicoletti, A. Loppini, L. Chiodo, V. Folli, G. Ruocco, and S. Filippi. Biophysical modeling of c. elegans neurons: Single ion currents and whole-cell dynamics of awcon and rmd. *PloS one*, 14(7):e0218738, 2019.

R. O'Hagan, M. Chalfie, and M. B. Goodman. The mec-4 deg/enac channel of caenorhabditis elegans touch receptor neurons transduces mechanical signals. *Nature neuroscience*, 8(1):43–50, 2005.

S. Onasch and J. Gjorgjieva. Circuit stability to perturbations reveals hidden variability in the balance of intrinsic and synaptic conductances. *Journal of Neuroscience*, 40(16): 3186–3202, 2020.

T. O'Leary, A. C. Sutton, and E. Marder. Computational models in the age of large datasets. *Current opinion in neurobiology*, 32:87–94, 2015.

R. Publio, R. F. Oliveira, and A. C. Roque. A realistic model of rod photoreceptor for use in a retina network model. *Neurocomputing*, 69(10-12):1020–1024, 2006.

D. Ramot, B. L. MacInnis, and M. B. Goodman. Bidirectional temperature-sensing by a single thermosensory neuron in c. elegans. *Nature neuroscience*, 11(8):908, 2008.

A. Roberts and B. M. Bush. *Neurones without impulses: their significance for vertebrate and invertebrate nervous systems*, volume 6. Cambridge University Press, 1981.

R. Sarpeshkar. Analog versus digital: extrapolating from electronics to neurobiology. *Neural computation*, 10(7):1601–1638, 1998.

G. Schilardi and S. Kleinlogel. Two functional classes of rod bipolar cells in the healthy and degenerated optogenetically treated murine retina. *Frontiers in Cellular Neuroscience*, 15, 2021.

D. J. Schulz, J.-M. Goaillard, and E. Marder. Variable channel expression in identified single and electrically coupled neurons in different animals. *Nature neuroscience*, 9(3): 356–362, 2006.

S. M. Silverstein, D. L. Demmin, J. B. Schallek, and S. I. Fradkin. Measures of retinal structure and function as biomarkers in neurology and psychiatry. *Biomarkers in Neuropsychiatry*, 2:100018, 2020.

W. Soofi, S. Archila, and A. A. Prinz. Co-variation of ionic conductances supports phase maintenance in stomatogastric neurons. *Journal of computational neuroscience*, 33(1): 77–95, 2012.

G. E. Stutzmann. Ryr2 calcium channels in the spotlight—i'm ready for my close up, dr. alzheimer! *Cell Calcium*, 94:102342, 2021.

C. Supnet and I. Bezprozvanny. The dysregulation of intracellular calcium in alzheimer disease. *Cell calcium*, 47(2):183–189, 2010.

X. Tong, Y. Ao, G. C. Faas, S. E. Nwaobi, J. Xu, M. D. Haustein, M. A. Anderson, I. Mody, M. L. Olsen, M. V. Sofroniew, et al. Astrocyte kir4. 1 ion channel deficits contribute to neuronal dysfunction in huntington's disease model mice. *Nature neuroscience*, 17(5): 694–703, 2014.

S. Usui, A. Ishihaiza, Y. Kamiyama, and H. Ishii. Ionic current model of bipolar cells in the lower vertebrate retina. *Vision research*, 36(24):4069–4076, 1996.

M. J. Van Hook, S. Nawy, and W. B. Thoreson. Voltage-and calcium-gated ion channels of neurons in the vertebrate retina. *Progress in retinal and eye research*, 72:100760, 2019.

C. Villa, H. Suphesiz, R. Combi, and E. Akyuz. Potassium channels in the neuronal homeostasis and neurodegenerative pathways underlying alzheimer's disease: An update. *Mechanisms of Ageing and Development*, 185:111197, 2020.

D. Waldner, N. Giraldo Sierra, S. Bonfield, L. Nguyen, I. Dimopoulos, Y. Sauvé, W. Stell, and N. Bech-Hansen. Cone dystrophy and ectopic synaptogenesis in a cacna1f loss of function model of congenital stationary night blindness (csnb2a). *Channels*, 12(1):17–33, 2018.

S. R. Williams, T. I. Toth, J. P. Turner, S. W. Hughes, and V. Crunelli. The 'window'component of the low threshold ca2+ current produces input signal amplification and bistability in cat and rat thalamocortical neurones. *The Journal of physiology*, 505 (3):689–705, 1997.

M. Yanagi, R. Joho, S. Southcott, A. Shukla, S. Ghose, and C. Tamminga. Kv3. 1-containing k+ channels are reduced in untreated schizophrenia and normalized with antipsychotic drugs. *Molecular psychiatry*, 19(5):573–579, 2014.

G. W. Zamponi, J. Striessnig, A. Koschak, and A. C. Dolphin. The physiology, pathology, and pharmacology of voltage-gated calcium channels and their future therapeutic potential. *Pharmacological reviews*, 67(4):821–870, 2015.

L. Zhang, X. Li, R. Zhou, and G. Xing. Possible role of potassium channel, big k in etiology of schizophrenia. *Medical hypotheses*, 67(1):41–43, 2006.

L. Zhang, Y. Zheng, J. Xie, and L. Shi. Potassium channels and their emerging role in parkinson's disease. *Brain Research Bulletin*, 160:1–7, 2020.